Modelling and characterisation of V_4C_3 precipitation and cementite dissolution during tempering of Fe–C–V martensitic steel

S. Yamasaki and H. K. D. H. Bhadeshia

The precipitation and Ostwald ripening behaviour of V_4C_3 (plate shaped) particles during the tempering of a ternary Fe–C–V martensitic steel have been characterised and modelled, taking account of local equilibrium, the capillarity effect, and simultaneous cementite enrichment and dissolution. Particles of V_4C_3 are represented as parabolic cylinders of revolution, with the tip radius chosen to yield the maximum lengthening rate. Transmission electron microscopy has been used to validate the theory; measurements of the average length, volume fraction, and number density of particles showed good agreement with experimental observations.   MST/5620

At the time the work was carried out the authors were in the Department of Materials Science and Metallurgy, University of Cambridge, Pembroke Street, Cambridge CB2 3QZ, UK. Mr Yamasaki (yamasaki@to.kimitsu.nsc.co.jp) is now with Nippon Steel Corp., 1 Kimitsu, Kimitsu-City, 299 1141 Japan. Manuscript received 15 August 2002; accepted 28 January 2003.

Nomenclature

a	activity
$c_V^{\alpha\beta}$	atomic fraction of vanadium in α in equilibrium with β
$c_{V,r}^{\alpha\beta}$	atomic fraction of vanadium in α in equilibrium with β at a curved interface
c_V^{θ}	atomic fraction of vanadium in θ
$\bar{c}_V$	atomic fraction of vanadium in the alloy
$\bar{d}$	mean diffusion distance between precipitates
d_t	thickness of a cementite particle
D_V	diffusion coefficient of vanadium
G^*	activation energy for nucleation
h	Planck constant
H	curvature of a particle
H^{SER}	enthalpy of the element or substance in the reference state at $25 \cdot 15°C$
I	nucleation rate
K	Boltzmann constant
N	number density of nucleation sites
N_A	Avogadro's number
N^{β}	number density of β precipitates
N_0^{β}	initial number density of β precipitates of the Ostwald ripening stage
$\bar{p}$	Péclet number
P	pressure
Q^*	activation energy for the transfer of atoms across the interface
r_c	critical tip radius at which growth ceases
r^{IC}	radius of curvature at the tip
r^*	nucleus size
r_0	initial average particle radius of the Ostwald ripening stage
t	time
T	absolute temperature
v	growth rate of a particle
v_c	growth rate of a flat interface governed by the interface process
Γ	capillarity coefficient
ξ_{θ}	volume fraction of θ phase
μ_X^{α}	chemical potential per X atom in α
μ_X^{β}	chemical potential per X atom in β
v^{β}	volume of an atom in β phase
σ	interfacial energy
Ω	supersaturation

Introduction

Alloy carbides have played an important role in the development of structural steels, for example, in the strengthening and toughening of microalloyed steels and in the exploitation of secondary hardened steels for service at elevated temperatures. A less well known application is when carbides, such as Mo_2C and V_4C_3 are introduced into the steel as hydrogen trapping sites to enhance the resistance to static fracture of components such as springs, bolts and power plant items.[1–3] The mechanical and hydrogen trapping properties depend on many parameters but the two most significant terms are the carbide size and number density. These parameters have in the past been manipulated on the basis of experience and experimental work. The aim in this research was to develop a model for estimating the kinetics of alloy–carbide microstructures during the tempering of steels, in the hope of accelerating the design process for novel, hydrogen resistant steels. As far as the authors are aware, there is no prior published work on the theory for the kinetics of martensite tempering, in which cementite gives way the precipitation and coarsening of alloy carbides.

In a previous report, a model for the precipitation of Mo_2C (needle shaped carbide) which accounts for local equilibrium, the capillarity effect, and simultaneous cementite enrichment and dissolution was presented.[4] However, V_4C_3 plays a more important role in enhancing the resistance to hydrogen embrittlement owing to its much higher hydrogen trapping capacity than Mo_2C (Ref. 5). Modelling of V_4C_3 precipitation is therefore useful for the development of hydrogen resistant steels. However, due to the plate shaped morphology, the model for V_4C_3 requires a modification from that for a needle shaped particle.

The purpose of the present work was to simulate the precipitation of V_4C_3 during the tempering of a martensitic steel in a Fe–C–V ternary system, taking account of local equilibrium, the capillarity effect, and at the same time, cementite enrichment and dissolution. The concepts of local equilibrium and the capillarity effect have been reviewed in previous work.[4]

Experimental work

Experiments were conducted to provide data for model verification. As shown later, the model can predict the average carbide length, volume fraction and number density. It is therefore necessary to obtain these data experimentally to verify the model. Transmission electron microscopy was used to obtain the necessary data.

MATERIAL

The chemical composition of the material designed for the present work was: Fe–0·10C–<0·005Si–1·99Mn–0·56V–0·03Al–0·0049N (wt-%). The steel was vacuum melted as a 10 kg ingot, heated at 1250°C for 30 min in an argon atmosphere, hot rolled to 12 mm thickness plate and air cooled. From this plate, the specimens for heat treatment were machined to 3 and 8 mm diameter. The specimens were sealed in silica tubes under a partial pressure of argon (∼150 mm Hg), before normalising. According to equilibrium calculations using MTDATA, the steel should be fully austenitic at temperatures above 1000°C. The homogenisation temperature was therefore chosen to be 1250°C, at which the specimens were held for 50 h.

After the homogenisation treatment, the specimens were quenched into water and the silica tubes were broken. The specimens were then sealed again and tempered at 600°C from 0·5 to 1160 h. After tempering, all specimens were again quenched into water, breaking the silica tubes.

SPECIMEN PREPARATION

Two types of specimens were examined using TEM: thin foils and carbon extraction replicas. Thin foil observation is crucial to define the orientation relationship between the precipitates and the matrix. Thin foils were sliced from bulk specimens as discs of diameter 3 mm and thickness ∼250 μm using a silicon carbide blade and cooling lubricant. After slicing, the specimens were ground with silicon carbide paper to around 50 μm thickness. Electropolishing was conducted using a twin jet electropolisher.[6] The solutions used for electropolishing were 8 vol.-% perchloric acid, 14 vol.-% glycerol and 78 vol.-% methanol. The electropolishing was performed with the solution at 15°C, the electrical potential being set at 50 V.

Carbon replica (single stage extraction) specimens were also prepared from each specimen. Specimens with 8 mm diameter were hot mounted with Bakelite moulding powder, and ground with silicon carbide paper down to 1200 grit and then polished with 6 and 1 μm diamond pastes. They were then chemically etched with 4 vol.-% nital for a few seconds. A carbon coating of 20–30 nm (brown gold colour) was deposited in a vacuum of 10^{-5} torr onto the etched surface. This film was then scored with a sharp blade to divide it into several smaller squares (∼1 mm²). Electrolytic etching in a solution of 5 vol.-% hydrochloric acid in methanol at 7·5 V was used to remove the carbon film, which was then washed in methanol and floated off in distilled water. These films were mounted on copper grids.

TEM OBSERVATION
Vanadium carbide

Figure 1 shows the thin foil TEM images of the specimens tempered for a variety of times. These pictures were taken from the [001] orientation of the matrix. Figure 2 shows the images of the specimen which was tempered 100 h. From the diffraction patterns in Fig. 2, these plate shaped precipitates have a face centred cubic (fcc) structure and are considered to be M_4C_3, where M stands for metal atoms (V, Fe, Mn). The chemical compositions of M_4C_3 particles were measured using energy dispersive spectroscopy using

carbon replica specimens; the average ratio of metallic elements is 0·975V : 0·018Fe : 0·007Mn. These precipitates are therefore virtually pure V_4C_3. It is known that V_4C_3 grows on the three equivalent $\{001\}_\alpha$ planes.[7] In Fig. 1, the needle like precipitates are the cross-section images of precipitates growing on the $\{001\}_\alpha$ plane, which is parallel to the observation direction.

Foil thickness

A knowledge of the thickness of the thin foil is necessary to estimate the volume fraction of V_4C_3. It was calculated using thickness fringes at the grain boundaries. The extinction distances for a two beam condition are known; it is therefore possible to calculate the thickness of the specimen by multiplying the extinction distance by the number of fringes. The thicknesses of the specimens were in this way found to be between 80 and 160 nm.

Carbide morphology and volume fraction

The V_4C_3 grows at the expense of cementite, on the $\{001\}_\alpha$ planes while keeping a plate shape whose average aspect ratio is 5 : 6. The carbide size was measured for each specimen from at least five different locations, each of which contained over 500 particles. The volume fraction was calculated using the length and thickness of each carbide particle and the foil thickness. The average carbide length, volume fraction, number density and number density distribution of the length of V_4C_3 particles are shown elsewhere in this paper along with the predictions made using the model.

Modelling of plate shaped carbide growth

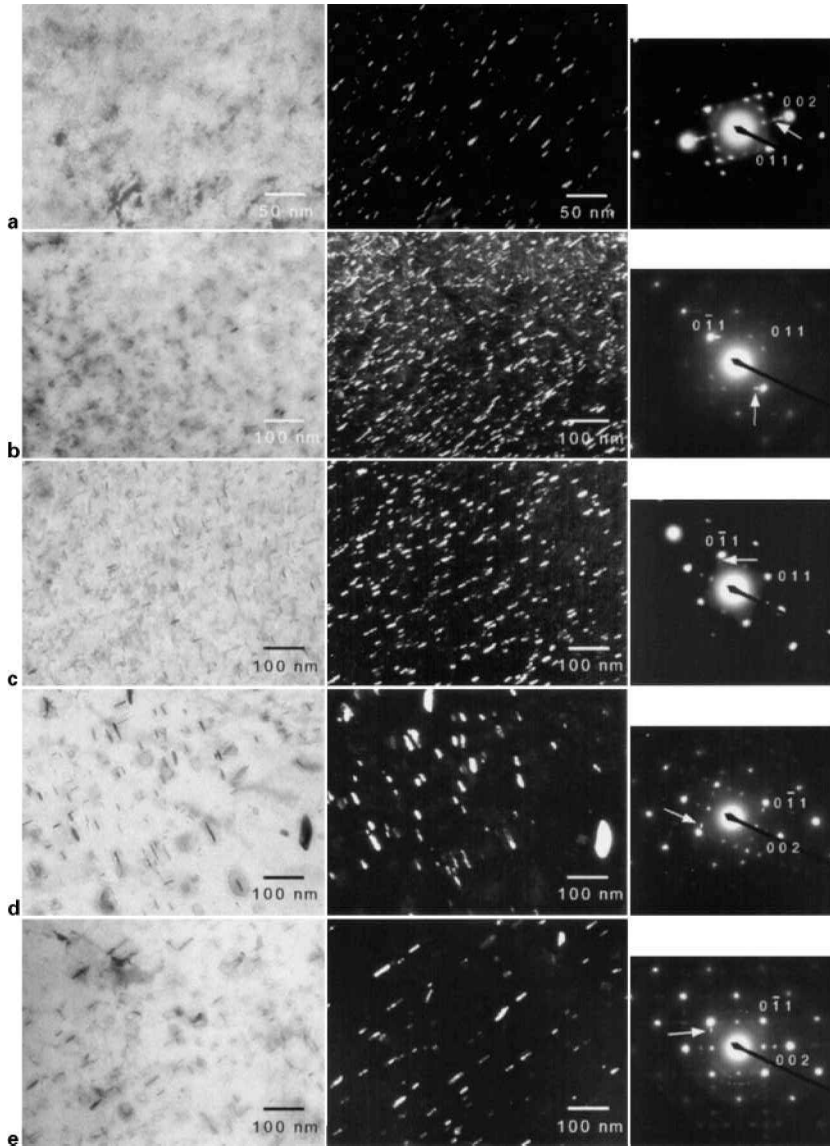### CHEMICAL COMPOSITION AND EQUILIBRIUM PHASES

Using MTDATA, the equilibrium phases and the compositions of the equilibrium carbides for the steel at a variety of temperatures were calculated. The calculation allowed for the potential existence of cementite, M_2C (hcp), M_4C_3 (fcc), M_7C_3, M_6C and $M_{23}C_6$ in addition to ferrite. According to the results, for 600°C, M_4C_3 (fcc) type carbide is the only stable carbide in this steel. The equilibrium composition of M_4C_3 according to MTDATA is 0·529V–0·450C–0·001Mn–0·000Fe–0·019N. It is therefore designated V_4C_3 in a Fe–C–V ternary system.

LOCAL EQUILIBRIUM, MULTICOMPONENT SYSTEMS

The concept of local equilibrium has been explained in previous work.[4] Particles of V_4C_3 precipitate from the matrix after the completion of paraequilibrium cementite precipitation. To satisfy the mass balances of V and C, the interfacial C concentration is assumed to be the same as that of the matrix.[8] However, it is strictly not the C concentration but the activity of C which should be identical for the ferrite/V_4C_3 interface and in the matrix far from the interface. If the interaction between C atoms and interstitial atoms is strong, e.g. for the case of C and Cr, the above assumption is not strictly valid. Figure 3 shows several isoactivity curves in the $\alpha + V_4C_3$ two phase field. As shown in Fig. 3, the deviation of the isoactivity curves from the isocarbon concentration lines (the perpendicular lines) is small and the above assumption is, therefore, considered to be valid.

CAPILLARITY EFFECT: MULTICOMPONENT SYSTEMS

When precipitates are curved the need to create interfaces affects local equilibrium, an effect which cannot be

a 10 h; *b* 30 h; *c* 100 h; *d* 560 h; *e* 1160 h

1 Observation (TEM) of test steel tempered at 600°C for different times: zone axis is [001] of ferrite; each dark field image was taken using diffraction spot shown by arrow

neglected when dealing with small particles or coarsening reactions.

If α and a parabolic cylinder of β are in contact at a curved interface then the conditions for local equilibrium are[9]

$$dT^\beta = dT^\alpha = dT \qquad \ldots \ldots \ldots \ldots \quad (1)$$

$$dP^\beta = dP^\alpha + \sigma \, dH \qquad \ldots \ldots \ldots \ldots \quad (2)$$

$$d\mu_1^\beta = d\mu_1^\alpha \quad d\mu_2^\beta = d\mu_2^\alpha \qquad \ldots \ldots \ldots \quad (3)$$

Here T, P, H, σ and μ represent temperature, pressure, curvature of β phase, surface energy, and chemical potential, respectively. If it is assumed that the pressure of the α phase is constant, from equation (2), the pressure change of the β phase can be represented as

$$\Delta P = \int_{P(H=0)}^{P} dP^\beta = \int_{H=0}^{H} \sigma \, dH = \frac{\sigma}{r^{IC}} \qquad \ldots \ldots \quad (4)$$
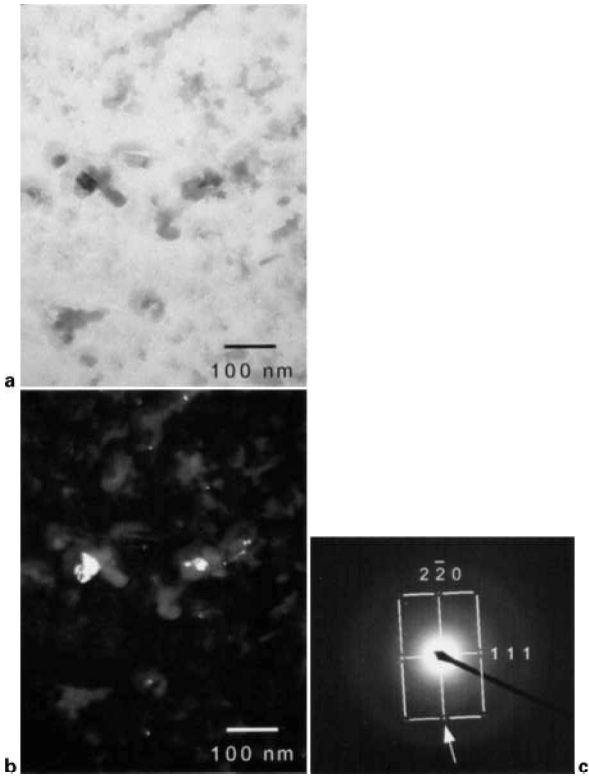
where r^{IC} is the radius of curvature at the tip. Accordingly, if the atomic volume of β is represented as v^β, an additional Gibbs energy term of $\delta \Delta G^\beta$ for a plate can be represented as

$$\Delta G^\beta = \Delta P v^\beta = \frac{\sigma v^\beta}{r^{IC}} \qquad \ldots \ldots \ldots \ldots \quad (5)$$

The simplest exact method to evaluate the influences of capillarity on the interface composition is to increase the Gibbs energy of the β phase in the database used by thermodynamical calculation software such as MTDATA. In MTDATA, the free energy of a phase such as ferrite is calculated using a sublattice model which involves terms called unaries. Commonly, the temperature and pressure dependence of unaries are described using the G-HSER format[10]

$$G^{T,P} - H^{SER} = a + bT + cT \ln T + eT^2 - fT^3 + i/T$$
$$- \int_0^P v^{PT} N_A \, dP \qquad (6)$$

where $G^{T,P}$ is the molar Gibbs energy at (T, P), $v^{P,T}$ is the atomic volume at (T, P), N_A is Avogadro's number and H^{SER} is the enthalpy of the element or substance in the reference state at 25·15°C. Although the data contained in the SGTE solutions and substances database do not include pressure dependent terms for most phases, it is possible to modify the database to add such terms. For example, in the case of V$_4$C$_3$ (fcc, a = 4·2 Å (0·42 nm)), the atomic volume $v^{V_4C_3}$ is $1·06 \times 10^{-29}$ m^3 and interfacial energy σ can be assumed to be 0·2 J m^{-2} (Ref. 11), and accordingly, the additional Gibbs energy would be 1274 J mol^{-1} for $\gamma^{IC} = 10$ Å

4   Composition of ferrite in equilibrium with V_4C_3 particle for several radius values taking into account capillarity effect: point b designates composition of ferrite matrix after completion of paraequilibrium cementite precipitation: 1 Å$=0.1$ nm

(1 nm). The database for the fcc phase (sublattice) was modified to add 1×10^{-6} J mol^{-1} per 1 Pa pressure increase.
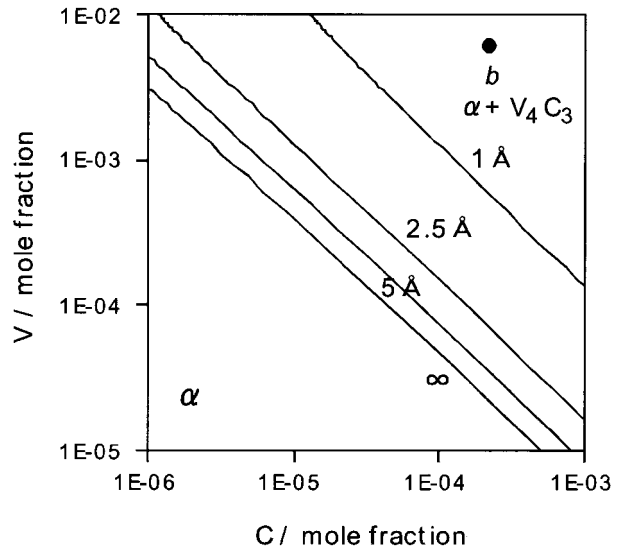
The capillarity effect on the interface composition $c_V^{\alpha V_4C_3}$, which is evaluated by increasing an additional Gibbs energy term in the database of MTDATA, is shown in Fig. 4 for several tip radii in $0.10C–0.56V$ (wt-%) steel.

GROWTH OF PARTICLES WITH CAPILLARITY EFFECT

From the observations made in the present work, V_4C_3 carbide particles with a fcc structure have been found to

3   Several isoactivity curves for C in $\alpha+V_4C_3$ two phase field: values in figure designate activity a of C; point b represents ferrite composition after completion of paraequilibrium precipitation

have a rectangular plate shape. A V_4C_3 particle can therefore be considered to be in the form of a plate.

Trivedi has given an exact solution for the diffusion problem which allows the composition to vary along the interface of a plate but assumes that the shape remains that of a parabolic cylinder.[12] In this theory, the capillarity effect and the interface kinetics effect are considered and it is found that the supersaturation can be represented as

$$\Omega = (\pi \bar{p}^{1/2})\, \exp(\bar{p})\, \mathrm{erfc}(\bar{p}^{1/2})$$
$$\times \left[1 + \frac{v}{v_c}\, \Omega S_1(\bar{p}) - \frac{r_c}{r^{IC}}\, \Omega S_2(\bar{p})\right] \qquad (7)$$
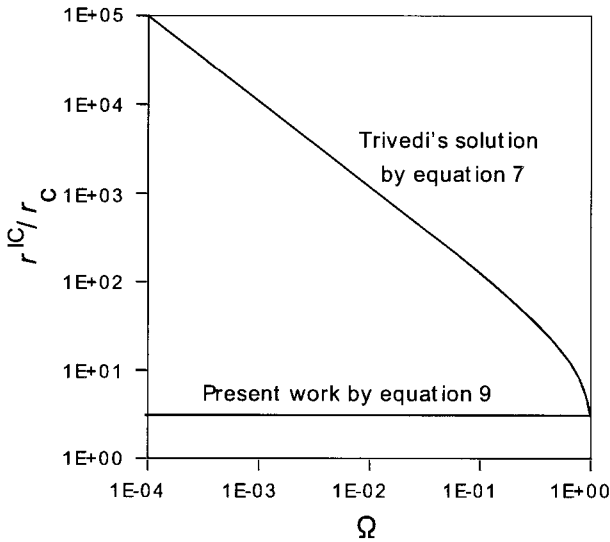
where Ω is the supersaturation, r^{IC} is the radius of curvature at the tip, r_c is the critical tip radius at which growth ceases, v is the lengthening rate, v_c is the velocity of a flat interface which is completely controlled by the interface processes, $\bar{p}$ is the Péclet number $\bar{p} = v r^{IC}/2D$ and $S_1(\bar{p})$ and $S_2(\bar{p})$ are

$$\left.\begin{array}{l} S_1(\bar{p}) = \frac{1}{2\bar{p}}\, M_1(\bar{p}) - 1 \\ S_2(\bar{p}) = \frac{1}{2\bar{p}}\, M_2(\bar{p}) - 1 \end{array}\right\} \quad . \quad . \quad . \quad . \quad . \quad . \quad . \quad . \quad (8)$$

The functions $M_1(\bar{p})$ and $M_2(\bar{p})$ were evaluated numerically by Trivedi and found to become $2/\pi$ and $4/\pi$ respectively, for small values of supersaturation $(\Omega < 1)$.[12] Equation (7) gives the general solution for the growth of precipitate plates. The right hand side is a sum of three terms of which the first is the result obtained by Ivantsov[13] for the case of the isoconcentrate boundary. The second and the third terms are corrections to that solution owing to the interface kinetics and capillarity effects respectively.

Equation (7) does not give a unique value of v or r^{IC}. The maximum growth rate hypothesis is therefore adopted to decide the growth rate and tip radius. The solution of equation (7) under the maximum growth rate hypothesis was obtained by Trivedi for large value of Ω $(\Omega \geqslant 0.2)$[12] and by Rivera-Díaz-del-Castillo for $\Omega \leqslant 0.2$.[14]

However, equation (7) gives huge values of the ratio r^{IC}/r_c at the maximum growth rate for small values of supersaturation Ω, e.g. $r^{IC}/r_c \approx 10^3$ at $\Omega = 10^{-2}$, $r^{IC}/r_c \approx 10^4$ at $\Omega = 10^{-3}$ as shown in Fig. 5.[14] The growing front of a particle has a large value of the radius and corresponding growth

5 Relationship between supersaturation Ω and ratio $r^{\mathrm{IC}}/r_{\mathrm{C}}$ for maximum growth rate of plates which is obtained by equations (7)[14] and equation (9)

rate is therefore extremely small in case of low supersaturation, by applying equation (7). As will be seen later, this is inconsistent with experimental data. An alternative approach due to Bolling and Tiller[15] was therefore adopted. Their method retains the parabolic shape with an assumed constant concentration at the interface appropriate to the tip radius. This means that if the interface effect can be neglected, the Péclet number is defined by[16]

$$\Omega = (\pi \bar{p})^{1/2} \exp(\bar{p}) \operatorname{erfc}\left(\bar{p}^{1/2}\right)$$
$$\times \left[1 + \frac{r_{\mathrm{c}}}{r^{\mathrm{IC}}} - \frac{\Omega}{(\pi \bar{p})^{1/2} \exp(\bar{p}) \operatorname{erfc}(\bar{p}^{1/2})} \right] \quad (9)$$

The maximum growth rate can be obtained by differentiating equation (9) with respect to r^{IC} and setting $\partial v / \partial r^{\mathrm{IC}} = 0$. The relationship between r^{IC} and r_{c}, which gives the maximum growth rate and supesaturation Ω satisfying equation (9), is shown in Fig. 5.

OVERALL TRANSFORMATION KINETICS

The carbide reaction during tempering in Fe−C−V steel, which includes the precipitation of V$_4$C$_3$, and the enrichment and dissolution of cementite, was simulated.

Enrichment and dissolution of cementite

Carbon is an interstitial solute in iron and hence has a much higher mobility than substitutional solutes or iron. It is natural therefore that iron carbides are the first to form when virgin martensite is tempered. In low and medium carbon steels containing dislocated martensite, cementite precipitates first in the tempering process. This cementite grows by a paraequilibrium mechanism; paraequilibrium is a state in which carbon achieves a uniform chemical potential across the interface subject to the constraint that the substitutional solute to iron atom ratio is maintained constant everywhere.[17] Thus, paraequilibrium cementite seems to form by a displacive mechanism.[18–21] The initial vanadium to iron atom ratio of the cementite is therefore assumed to be the same as that given by the average chemical composition.[17]

During tempering, vanadium diffuses into the cementite to enrich it towards equilibrium, and at some stage, the cementite begins to dissolve to give way to the precipitation of the more stable V$_4$C$_3$. The volume fraction of cementite can be calculated using the lever rule and assuming that any

residual carbon concentration in the ferrite is so small that it can be neglected. The volume fraction of cementite ξ_θ is then given by[22]

$$\varsigma_\theta = 1 \cdot 0065 \times \frac{\bar{c}}{c^{\theta \alpha}} \quad c^{\theta \alpha} \approx 0 \cdot 25 \quad . \quad . \quad . \quad . \quad . \quad (10)$$

by taking account of the difference in ferrite and cementite densities. From TEM observations, the average thickness of a cementite plate is $\sim 2 \times 10^{-8}$ m in the grains and 5×10^{-8} m on the grain boundaries.

The rate of enrichment is given approximately by[23]

$$c_{\mathrm{V}}^{\theta} = \bar{c}_{\mathrm{V}} + 4(D_{\mathrm{V}} t)^{1/2} \frac{\bar{c}_{\mathrm{V}} - c_{\mathrm{V}}^{\alpha \theta}}{d_{\mathrm{t}} \, \pi^{1/2}} \quad . \quad . \quad . \quad . \quad (11)$$

where c_{V}^{θ} represents the atomic fraction of V in cementite, t is the time since cementite formation, d_{t} is the thickness of the cementite plate, D_{V} is the diffusion coefficient of V in the matrix (it is assumed that the corresponding diffusivity in the cementite is identical to that in the ferrite), $c_{\mathrm{V}}^{\alpha \theta}$ is the atomic fraction of V in the ferrite which is in equilibrium with the cementite, and $\bar{c}_{\mathrm{V}}$ is the mean atomic fraction of V in the alloy.

It is assumed that cementite dissolves in the manner described by Robson and Bhadeshia[24] by which the dissolution rate v_θ is determined as

$$v_\theta = -\frac{D_{\mathrm{V}}}{\bar{d}} \frac{c_{\mathrm{V}}^{\alpha \theta} - c_{\mathrm{V}}^{\alpha \mathrm{V}_4 \mathrm{C}_3}}{c_{\mathrm{V}}^{\theta \alpha} - c_{\mathrm{V}}^{\alpha \theta}} \quad . \quad . \quad . \quad . \quad . \quad (12)$$

where $\bar{d}$ is the mean diffusion distance between θ and V$_4$C$_3$ precipitates, given by

$$\bar{d} = (N^\theta + N^{\mathrm{V}_4 \mathrm{C}_3})^{-1/3} \quad . \quad . \quad . \quad . \quad . \quad . \quad (13)$$

where N^θ and $N^{\mathrm{V}_4 \mathrm{C}_3}$ are the number densities of θ and V$_4$C$_3$ particles respectively.

Nucleation of V$_4$C$_3$

The nucleation rate of V$_4$C$_3$ particles is given as

$$I = N \frac{kT}{h} \exp\left[\frac{-(G^* + Q^*)}{kT} \right] \quad . \quad . \quad . \quad . \quad (14)$$

where N is the number of nucleation sites per unit volume of the system, Q^* is the free energy of activation for the transfer of atoms across the interface (approximately equal to the activation energy for diffusion when the nucleus is coherent), k is the Boltzmann constant and h is the Planck constant.[25] The activation energy for nucleation is G^* and is represented as

$$G^* = \frac{16\pi}{3} \frac{\sigma^3}{\Delta G_{\mathrm{V}}^2} \quad . \quad . \quad . \quad . \quad . \quad . \quad . \quad (15)$$

where ΔG_{V} is the chemical free energy change per unit volume of nuclei and has a negative value. Each critical sized embryo can be made supercritical by transferring an atom in contact with the embryo into it; it then becomes a nucleus. The nucleus size is represented as

$$r^* = -\frac{2\sigma}{\Delta G_{\mathrm{V}}} \quad . \quad . \quad . \quad . \quad . \quad . \quad . \quad (16)$$

ΔG_{V} is calculated using MTDATA as $-2 \cdot 387 \times 10^9$ J m^{-3}. This value is for the beginning of precipitation of V$_4$C$_3$ and it will decrease as the precipitation proceeds. The change of the value of ΔG_{V} is calculated corresponding to the progress of the precipitation reaction using a mean field approximation, i.e. assuming that the solute is distributed uniformly in the matrix.

Diffusion controlled growth with capillarity

Modelling of the local equilibrium of V$_4$C$_3$ precipitation is based on Coates' diffusion controlled growth theory[8] accounting for the capillarity effect. The critical radius of

curvature r_c at which growth ceases was calculated using MTDATA, with a modification to the database of the fcc phase to include a pressure change. The growth rate of particles is the maximum rate for given values of the carbon concentration in the matrix and the supersaturation Ω of V. The growth rate obtained from the values of $\bar{p}$ and the ratio r^{IC}/r_c corresponding to the maximum growth rate satisfies equation (9).

Ostwald ripening of particles

Coarsening occurs because the total energy of the system is reduced by eliminating interfaces; in practice, large particles grow more rapidly than small particles during precipitation, and large particles grow at the expense of smaller ones during classical coarsening. The average particle size therefore increases with time. Classical coarsening occurs slowly because of the small energies associated with the interfaces compared with the free energy change accompanying precipitation. Ostwald ripening can therefore be assumed to occur after the 'completion' of the precipitation of V$_4$C$_3$.

The combination of nucleation and growth described in the earlier part of this paper gives rise to a distribution of V$_4$C$_3$ lengths, but for a given supersaturation, they all have the same tip radius. An approximate treatment, in which a V$_4$C$_3$ particle is modelled to be a plate of which the periphery is hemicylindrical, was therefore adopted for the Ostwald ripening stage, after the completion of precipitation. The growth (or dissolution) rate can be calculated using Zener's theory as

$$v = -\frac{D_V}{\bar{d}} \frac{\bar{c}_V - c_{V,r}^{\alpha V_4 C_3}}{c_V^{V_4 C_3 \alpha} - c_{V,r}^{\alpha V_4 C_3}} \quad \text{. . . . . (17)}$$

where $c_{V,r}^{\alpha V_4 C_3}$ is the equilibrium concentration of vanadium in ferrite at the hemicylindrical tip of a V$_4$C$_3$ particle and $\bar{d}$ is the mean diffusion distance between particles, which can be, represented as[24]
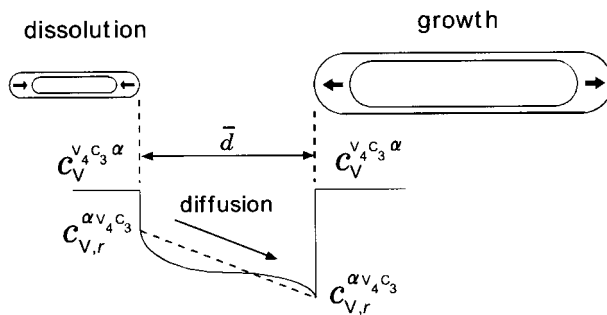
$$\bar{d} = (N^\beta)^{-1/3} \quad \text{. . . . . (18)}$$

where N^β is the number density of V$_4$C$_3$ particles. The interfacial composition at the hemicylindrical tip of particles can be calculated by an analogous method for the capillarity effect, which is explained above.

During Ostwald ripening, particles in general should become spheroidised to reduce the surface area if the interfacial energy is not orientation dependent. However, the aspect ratio of V$_4$C$_3$ particles does not in fact change significantly. These particles are found to grow whilst retaining the plate shape as shown in Fig. 1. It is therefore assumed that the shape of particles was preserved during Ostwald ripening. Accordingly, particles grow or dissolve as shown in Fig. 6.

Inputs and calculations

The precipitation calculations were done in steps of 100 s, and in each step, the nucleation rate, nucleus size which was the initial size of particle growth, growth rate, the V and C concentration change in the matrix corresponding to the growth of V$_4$C$_3$, and the enrichment and dissolution of cementite were calculated. The consumption of nucleation sites during the transformation was accounted for in each step. Once the concentrations of V and C in the matrix ($\bar{c}_V$ and $\bar{c}_C$) were determined, the corresponding supersaturations of V (Ω_V) and the critical radius r_c were obtained. Once Ω_V and r_c were obtained, the value of $\bar{p}$ which satisfies equation (9), and finally, the maximum growth rate and the tip radius of a V$_4$C$_3$ particle r^{IC} which gave the maximum rate for the corresponding value of $\bar{p}$ could be calculated. The volume of each particle was calculated as a parabolic cylinder.

6 Schematic drawing of Ostwald ripening of plate shaped particles

After the completion of the precipitation and growth stage, each V$_4$C$_3$ particle was modelled to be a plate of which the periphery is hemicylindrical for the Ostwald ripening stage. In this stage, $c_{V,r}^{\alpha V_4 C_3}$ at the tip of each plate shaped particle were calculated, and then the growth (or dissolution) rates at the tip were calculated.

The parameters used in the calculations are listed in Table 1. The nucleation site density was obtained by fitting with experimental data. The V$_4$C$_3$/ferrite interface energy,[11] and the diffusivity of vanadium in ferrite[26] were obtained from the literature.
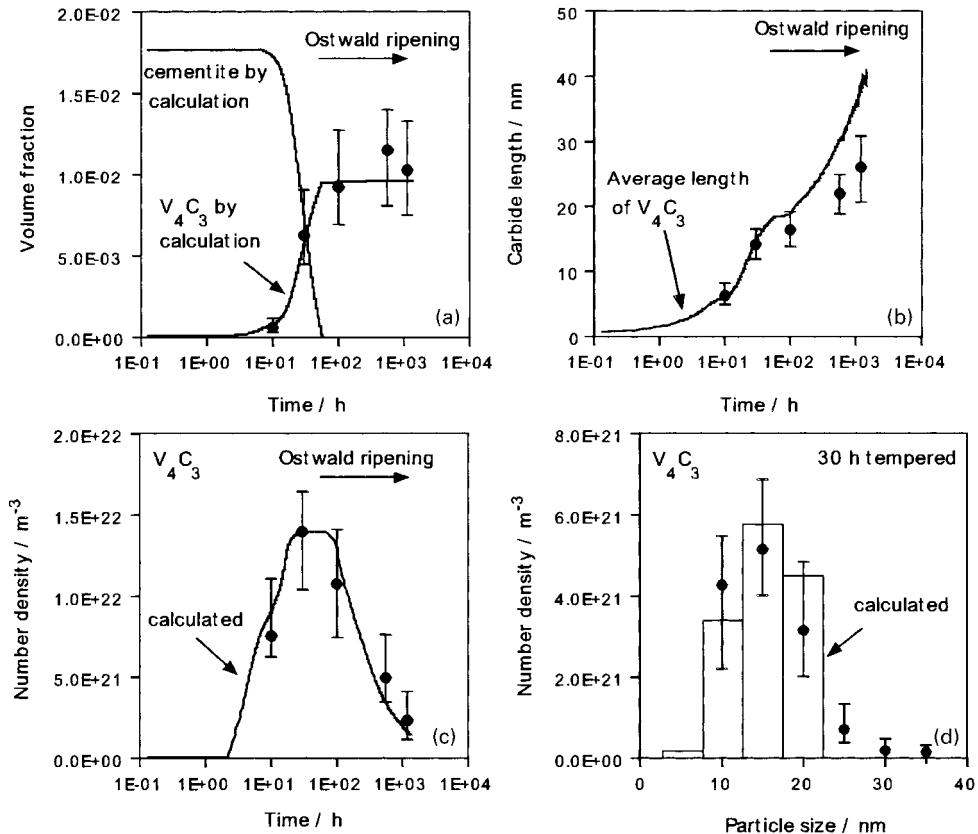
Results

Figure 7 shows the comparisons of the calculations and the experimental observations. Experimental data were obtained from several areas in each specimen. In Fig. 7, the solid circles represent the average of data from different areas, and the scatter of the data is indicated by an error bar. The technique allows the carbide dimensions to be measured to an accuracy of ± 1 nm. There have been attempts to characterise vanadium carbide, e.g. the lattice structure,[27–29] morphology,[28–30] average size[30,31] and size distribution.[31] However, the variation of these characteristics of vanadium carbides with tempering time through the nucleation and growth stages to the Ostwald ripening stage has not been measured in detail.

After the completion of paraequilibrium cementite precipitation, the concentration of carbon in the matrix is quite low (0·022 at.-%, according to MTDATA). Carbon atoms, which are necessary for the precipitation of V$_4$C$_3$, are provided by the dissolution of cementite. After the completion of precipitation, Ostwald ripening proceeds with a constant volume fraction of V$_4$C$_3$. Figure 7a shows such simultaneous V$_3$C$_4$ precipitation and cementite dissolution

Table 1 Calculation parameters for precipitation of carbides in ternary system (Fe–0·10C–0·56V, wt-%)

Parameter	Value
Shape	Plate
Tempering temperature	600°C
Surface energy of V$_4$C$_3$	0·2 J m^{-2}
Driving force for nucleation of V$_4$C$_3$	$-2·387 \times 10^9$ J m^{-3}
Nucleation site density of V$_4$C$_3$	$1·48 \times 10^{22}$ m^{-3}
Maximum volume fraction of cementite	$1·796 \times 10^{-2}$
Maximum volume fraction of V$_4$C$_3$	$9·66 \times 10^{-3}$
Atomic fraction $c_V^{\alpha\theta}$	$4·356 \times 10^{-3}$
Atomic fraction $c_V^{\theta\alpha}$	$1·063 \times 10^{-1}$
Atomic fraction $c_V^{\alpha V_4 C_3}$	$9·620 \times 10^{-4}$
Atomic fraction $c_V^{V_4 C_3 \alpha}$	$5·320 \times 10^{-1}$
Thickness of cementite in grains	$2·0 \times 10^{-8}$ m
Thickness of cementite on grain boundaries	$5·0 \times 10^{-8}$ m
Diffusion constant of V D_V	$3·05 \times 10^{-4}$ m^2 s^{-1}
Activation energy for V diffusion Q_V	$2·39 \times 10^5$ J mol^{-1}

a relationship between volume fraction of V$_4$C$_3$ particles and tempering time; *b* relationship between average length of V$_4$C$_3$ particles and tempering time; *c* relationship between number density of V$_4$C$_3$ particles whose size are over 4 nm and tempering time; *d* number density distribution of the length of V$_4$C$_3$ particles for 30 h tempered steel

7 Comparisons between calculations and observations

behaviour. From the observations and calculations, the volume fraction of V$_4$C$_3$ increases with time up to 60 h and then remains constant, as shown in Fig. 7*a*. It is therefore considered that nucleation and growth stage ends at ∼60 h and the Ostwald ripening stage commences after that.

The average length of V$_4$C$_3$ particles increases during the precipitation and growth stage. During the Ostwald ripening stage, the aspect ratio of particles was fixed and the growth rate (or dissolution rate) of each particle was calculated using the tip radius of the edges of the plate. As an average, the length therefore increases during Ostwald ripening as shown in Fig. 7*b*.

The number density of V$_4$C$_3$ particles whose length is over 4 nm was calculated, as shown in Fig. 7*c*, for comparison with observation; V$_4$C$_3$ particles of size less than 4 nm could not easily be observed using conventional TEM. During the Ostwald ripening stage, the number density decreases.

The calculated number density distribution of the length of V$_4$C$_3$ particles is shown in Fig. 7*d* for the tempering time of 30 h. Each point which is placed at the length of X nm represents the number density of the observed particles whose length is from $(X-2 \cdot 5)$ nm to $(X+2 \cdot 5)$ nm.

The calculations in general agree well with the observations. However, there are discrepancies between calculations and observations for the average length of V$_4$C$_3$ particles during Ostwald ripening. It was observed that particles of V$_4$C$_3$ kept their shape in the laths, however, they were spheroidised on the lath boundaries or the grain boundaries. Since the observations contain information from the particles in the grains and on the grain boundaries, the average length of V$_4$C$_3$ particles is smaller than predicted by the calculations during Ostwald ripening.

Discussion

The reason why the precipitates retain their shape during coarsening is now discussed. The orientation relationship between V$_4$C$_3$ and the ferrite matrix is reported as[27,32]
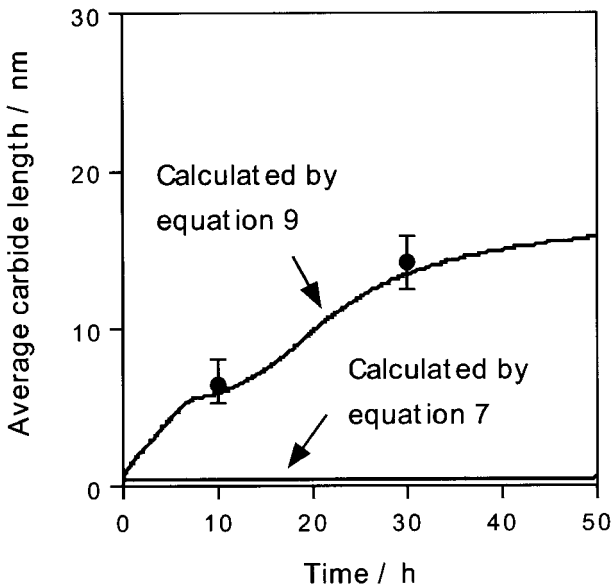
$$\{100\}_{\mathrm{V_4C_3}}//\{100\}_\alpha \quad <010>_{\mathrm{V_4C_3}}//<011>_\alpha \qquad (19)$$

V$_4$C$_3$ is formed as platelets lying on $\{100\}_\alpha$ planes. The configuration of V and Fe atoms in $\{100\}_\alpha$ planes indicates excellent coherency between both lattices (∼2·1% mismatch). On the contrary, lattice misfit is ∼30% in planes perpendicular to this plane.[7] This is the primary reason that V$_4$C$_3$ grows easily as thin plates. In other words, the interfacial energy is orientation dependent.

For the precipitation and growth stage, Trivedi's theory for the growth of the plate shaped particles was not adopted; it is not valid because of the large value of $r^{\mathrm{IC}}/r_{\mathrm{c}}$ for the small supersaturation. Instead of Trivedi's theory, which allows the composition to vary along the interface of a plate, the composition was assumed to be constant at the interface in the present model. Figure 8 shows the comparisons of the calculated average length of particles obtained by Trivedi's theory and the present model, along with experimental data. There is a large discrepancy between the observations and calculations using Trivedi's theory.

For the Ostwald ripening stage, V$_4$C$_3$ particles were modelled as plates with hemicylindrical ends. Coarsening theory for spheres leads to the following relationship[33,34]

$$r^3 - r_0^3 = \left(\frac{8\sigma v^\beta D_{\mathrm{VC}} c_{\mathrm{V}}^{\alpha\beta}}{9kT}\right) t \qquad \ldots \ldots \ldots \quad (20)$$

8 Comparisons between calculated average length of particles obtained using equation (7) and present model and observations

9 Comparisons of number density of V_4C_3 particles calculated as plate shaped and as spherical and calculated using equation (21)

where r is the average radius, r_0 is the initial average particle radius and t is time. During Ostwald ripening, the volume fraction of V_4C_3 can be assumed to be constant. The number density of V_4C_3 can be therefore represented as

$$N^{V_4C_3} = N_0^{V_4C_3} \frac{r_0^3}{r_0^3 + \frac{8\sigma v^\beta D_V c_V^{\alpha\beta}}{9kT} t} \qquad . \quad . \quad . \quad . \quad . \quad . \quad (21)$$

where $N_0^{V_4C_3}$ is the initial number density of V_4C_3 particles when the Ostwald ripening stage starts. Figure 9 shows that similar results are obtained for the number densities, both for the sphere and plate morphologies, and for equation (21).
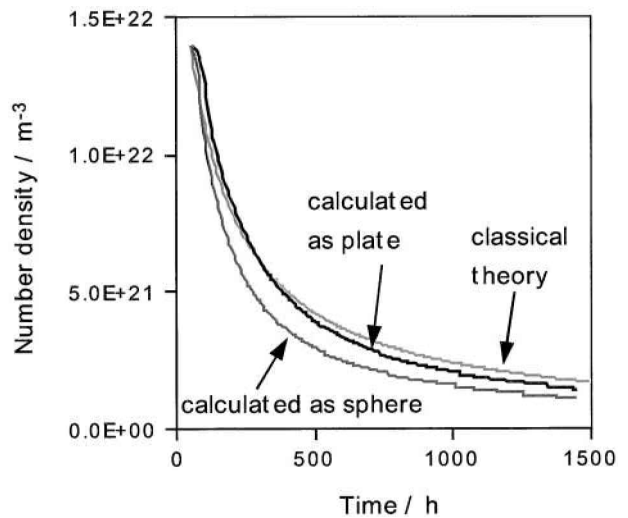
Summary and conclusions

The precipitation and Ostwald ripening behaviour of V_4C_3 (plate shaped) particles during the tempering of a ternary Fe–C–V martensitic steel have been characterised and modelled, taking account of local equilibrium, the capillarity effect, and simultaneous cementite enrichment and dissolution.

In conclusion, by modelling a V_4C_3 particle as a parabolic cylinder with a constant concentration of the solute along the surface of the tip, and assuming that growth occurs at a maximum rate, the model has been shown to be capable of estimating the average length, volume fraction, and number density of particles in a manner consistent with experimental observations. The growth rate depends on the supersaturation of vanadium (Ω_V) and the ratio of the solute concentration in the matrix $\bar{c}_V/\bar{c}_C$.

Acknowledgements

References

1. N. IBARAKI, A. INADA, M. SHIMOTSUSA, T. NAKAYAMA, T. IWATA and M. NAGAO: *Kobelco Technol. Rev.*, 1998, **21**, 21–25.
2. S. YAMASAKI, M. KUBOTA and T. TARUI: *Nippon Steel Tech. Rep.*, 1999, **80**, 50–55.
3. T. KUSHIDA, N. KURATOMI, T. KUDOH, H. MATSUMOTO, T. TSUMURA and F. NAKASATO: *Tetsu-to-Hagane (J. Iron Steel Inst. Jpn)*, 1996, **82**, 297–302.
4. S. YAMASAKI and H. K. D. H. BHADESHIA: *Mater. Sci. Technol.*, 2002, **19**, 723–731.
5. S. YAMASAKI: CPGS thesis, University of Cambridge, UK, 2001.
6. P. M. KERRY and J. NUTTING: *J. Iron Steel Inst.*, 1959, **192**, 246–248.
7. M. TANINO: Proc. Int. Conf. on 'Phys. metall. thermomech. process steels other met.', Vol. 1, 70–79; 1988.
8. D. E. COATES: *Metall. Trans.*, 1972, **3**, 1203–1212.
9. R. T. DEHOFF: 'Thermodynamics in materials science', 378; 1993, New York, NY, McGraw–Hill.
10. S. M. HODSON: 'MTDATA – metallurgical and thermochemical databank'; 1989, Teddington, National Physical Laboratory.
11. D. A. PORTER and K. E. EASTERLING: 'Phase transformations and alloys', 2nd edn, 147; 1992, London, Chapman and Hall.
12. R. TRIVEDI: *Metall. Trans.*, 1970, **1**, 921–927.
13. G. P. IVANTSOV: *Dolk. Akad. Nauk. SSSR*, 1947, **58**, 567–569.
14. P. E. J. RIVERA-DÍAZ-DEL-CASTILLO and H. K. D. H. BHADESHIA: *Mater. Sci. Technol.*, 2001, **17**, 25–29.
15. G. F. BOLLING and W. A. TILLER: *J. Appl. Phys.*, 1961, **32**, 2587–2605.
16. J. W. CHRISTIAN: 'The theory of transformations in metals and alloys', 2nd edn, Part 1, 498; 1975, Oxford, Pergamon Press.
17. A. HULTGREN: *Trans. ASM*, 1968, **39**, 915–1005.
18. H. K. D. H. BHADESHIA: 'Bainite in steels', 2nd edn, 63; 2001, London, IoM Communications.
19. S. S. BABU, K. HONO and T. SAKURAI: *Appl. Surf. Sci.*, 1993, **67**, 321–327.
20. R. C. THOMSON and M. K. MILLER: *Appl. Surf. Sci.*, 1995, **87–88**, 185–193.
21. R. C. THOMSON and M. K. MILLER: *Acta Metall.*, 1998, **46**, 2203–2213.
22. M. TAKAHASHI and H. K. D. H. BHADESHIA: *Mater. Sci. Technol.*, 1990, **6**, 592–603.
23. H. K. D. H. BHADESHIA: *Mater. Sci. Technol.*, 1989, **5**, 131–137.
24. J. D. ROBSON and H. K. D. H. BHADESHIA: *Mater. Sci. Technol.*, 1997, **13**, 631–639.
25. J. W. CHRISTIAN: 'The theory of transformations in metals and alloys', 2nd edn, Part 1, 441; 1975, Oxford, Pergamon Press.
26. W. BOWEN and G. M. LEAK: *Metall. Trans.*, 1970, **1**, 1695–1700.
27. R. G. BAKER and J. NUTTING: *ISI Special Report*, 1959, **64**, 1.
28. Y. I. USTINOVSHCHIKOV: *Metal Sci.*, 1984, **18**, 337–344.

29. M. TANINO and T. NISHIDA: *J. Jpn Inst. Met.*, 1965, **29**, 794−800.
30. T. HARA, T. TSUCHIDA and K. TSUZAKI: *CAMP−ISIJ*, 2001, **14**, 641.
31. G. L. DUNLOP and R. W. K. HONEYCOMBE: *Metal Sci*, 1978, **12**, 367−671.

32. E. TEKIN and P. M. KELLY: *J. Iron Steel Inst.*, 1965, **203**, 715.
33. M. LIFSHITZ and V. V. SLYOZOV: *J. Phys. Chem. Solids*, 1961, **19**, 35−50.
34. R. WARGNER and R. KAMPMANN: 'Materials science and technology', Vol. 5, 213−303; 1991, Weinheim, VCH.